Geoderma 370 (2020) 114356

Contents lists available at ScienceDirect

Geoderma

journal homepage: www.elsevier.com/locate/geoderma

Low-field magnetic resonance imaging of roots in intact clayey and silty soils

G. Cody Bagnall[a,*], Neha Koonjoo[b,c,d], Stephen A. Altobelli[e], Mark S. Conradi[e], Eiichi Fukushima[e], Dean O. Kuethe[e], John E. Mullet[f], Haly Neely[g], William L. Rooney[g], Karl F. Stupic[h], Brock Weers[f], Bo Zhu[b,c,d], Matthew S. Rosen[b,c,d,1], Cristine L.S. Morgan[i,1]

[a] Department of Biological and Agricultural Engineering, Texas A&M University, College Station, TX, USA
[b] Athinoula A. Martinos Center for Biomedical Imaging, Department of Radiology, Massachusetts General Hospital, Charlestown, MA 02129, USA
[c] Harvard Medical School, Boston, MA 02115, USA
[d] Department of Physics, Harvard University, Cambridge, MA 02138, USA
[e] ABQMR, Inc. 2301 Yale Blvd SE, Suite C2, Albuquerque, NM 87106, USA
[f] Department of Biochemistry and Biophysics, Texas A&M University, College Station, TX, USA
[g] Department of Soil and Crop Science, Texas A&M University, College Station, TX, USA
[h] National Institute of Standards and Technology, Applied Physics Division, 325 Broadway, Boulder, CO 80305, USA
[i] Soil Health Institute, 2803 Slater Road. Suite 115, Morrisville, NC 27560, USA

ARTICLE INFO

Handling Editor: Yvan Capowiez

ABSTRACT

The development of a robust method to non-invasively visualize root morphology in natural soils has been hampered by the opaque, physical, and structural properties of soils. In this work we describe a novel technology, low field magnetic resonance imaging (LF-MRI), for imaging energy sorghum (*Sorghum bicolor* (L.) Moench) root morphology and architecture in intact soils. The use of magnetic fields much weaker than those used with traditional MRI experiments reduces the distortion due to magnetic material naturally present in agricultural soils. A laboratory based LF-MRI operating at 47 mT magnetic field strength was evaluated using two sets of soil cores: 1) soil/root cores of Weswood silt loam (Udifluventic Haplustept) and a Belk clay (Entic Hapluderts) from a conventionally tilled field, and 2) soil/root cores from rhizotrons filled with either a Houston Black (Udic Haplusterts) clay or a sandy loam purchased from a turf company. The maximum soil water nuclear magnetic resonance (NMR) relaxation time T_2 (4 ms) and the typical root water relaxation time T_2 (100 ms) are far enough apart to provide a unique contrast mechanism such that the soil water signal has decayed to the point of no longer being detectable during the data collection time period. 2-D MRI projection images were produced of roots with a diameter range of 1.5–2.0 mm using an image acquisition time of 15 min with a pixel resolution of 1.74 mm in four soil types. Additionally, we demonstrate the use of a data-driven machine learning reconstruction approach, Automated Transform by Manifold Approximation (AUTOMAP) to reconstruct raw data and improve the quality of the final images. The application of AUTOMAP showed a SNR (Signal to Noise Ratio) improvement of two fold on average. The use of low field MRI presented here demonstrates the possibility of applying low field MRI through intact soils to root phenotyping and agronomy to aid in understanding of root morphology and the spatial arrangement of roots *in situ*.

1. Introduction

Analysis of plant root system development and architecture in structured field soils is challenging. Technology that enables *in situ* root system measurement and analysis would improve our understanding of the development, architecture, and responses to environmental variation, and improve root models, breeding for ideal root structures, and management decisions that focus on carbon sequestration in soil (Lynch, 1995, 2018; Zhu, et al., 2011). While many tools have been developed for laboratory-based measurements (Armengaud et al., 2009;

Abbreviations: LF-MRI, Low Field Magnetic Resonance Imaging; HF-MRI, High Field Magnetic Resonance Imaging; MR, Magnetic Resonance; MRI, Magnetic Resonance Imaging; NMR, Nuclear Magnetic Resonance; RF, Radio Frequency; SNR, Signal to Noise Ratio; AUTOMAP, Automated Transform by Manifold Approximation; OD, Outside Diameter; AWG, American Wire Gauge; IFFT, Inverse Fast Fourier Transform; FFT, Fast Fourier Transform

* Corresponding author.
E-mail address: gcbagnall@outlook.com (G.C. Bagnall).
[1] Both authors contributed equally.

https://doi.org/10.1016/j.geoderma.2020.114356
Received 8 November 2019; Received in revised form 25 March 2020; Accepted 27 March 2020

Mooney et al., 2012; Xhou and Luo, 2009), no current technology is capable of in-field, *in situ* measurements of root systems across a variety of agricultural soils. This paper presents a proof-of-concept of a system capable of imaging plant roots *in situ* growing in agriculturally relevant soils.

The most common method for quantifying root systems is by excavation, washing and imaging the cleaned roots, often called "shovelomics". Trachsel et al. (2011) gives an example of this method, in which the roots are excavated and visual metrics are used to describe the roots in ways that advise plant breeding applications. Newer methods that have varying adoptions by researchers include 2-D flatbed optical scanners (Araujo et al., 2004), X-ray computed tomography (Flavel et al., 2012, 2017; Lafond et al., 2015), and magnetic resonance imaging (MRI) (Atkinson et al., 2019; Jahnke et al., 2009; Koch et al., 2019; Metzner et al., 2014). Flatbed optical scanners are useful for imaging roots after removal of soil but are not suitable for *in situ* measurements. X-ray computed tomography is a high-resolution technique that is useful in a laboratory setting, but safe field deployment is difficult. Several researchers have used MRI in laboratory settings to image plant root architecture in re-packed soil and engineered potting media and soil mixes. Laboratory based plant root system morphometric analysis is useful; however, these systems do not accurately reflect the root system architectures found in field soils (Zhu, et al., 2011).

Magnetic resonance imaging can be categorized based on the magnetic field strength operational range, with high field MRI (HF-MRI) typically performed in the range of 1–10 T (Tesla) and low field MRI (LF-MRI) operating below 1 T. The source of the signal in the MRI experiment in both cases is nuclear magnetic resonance (NMR) inductive detection of precessing nuclear magnetic moments in a magnetic field. Spatial encoding is obtained by phase and frequency modulating the detected signal using the application of magnetic gradient fields to the system. Systems of precessing nuclear magnetic moments can be characterized by their NMR properties. In particular the time for spin systems to revert to their thermal equilibrium polarization is known as the spin lattice relaxation time (T_1) and the time for precsssing magnetization to become dephased is the spin–spin relaxation time (T_2). In MRI, time constants T_1 and T_2 can be used to provide image contrast, and differences in these values allow a target material to be separated from the background material surrounding the desired target (Hall et al., 1997).

Magnetic resonance imaging, as performed in this work, images ^{1}H nuclear spins which in the case of soil and roots, are found in the form of water. The amount of water that is found in soil changes with the amount of silicate clay in the soil matrix as well as the relative soil moisture content. Soil water has been found to have short T_2 relaxation times (Hall et al., 1997), and is dependent on soil type (Hall et al., 1997; Votrubova et al., 2000). The soil-dependent T_1 and T_2 influence the imaging strategy which requires the relaxation time to be measured for each soil (Prebble and Currie, 1970). In the case of root imaging in soil, the greater the difference between the soil water relaxation time and the root water relaxation time, the easier it is to distinguish roots from soil.

To differentiate between soil water and water located in the roots, we need to understand the relaxation times of each. Rogers and Bottomley (1987) discovered a clear distinction between soil water and root water relaxation times and conclude that soil texture and water potential need to be considered for future use of MRI systems in soils-based research. In that work, fava beans were grown in eight natural soils with a range of clay contents, and eight potting media. The samples were placed in a 1.5 T field to measure soil water and for root imaging. Natural soils with more than 4% paramagnetic material did not produce usable images at 1.5 T. The images produced from soils with less than 4% paramagnetic material, such as some of the manufactured potting media and some of the natural soils, produced mixed results with some generating clear root images and others, such as the Houston Black clay, producing distorted images. Since most soils are described in terms of soil texture instead of paramagnetic content, Pflugfelder et al. (2017) used some of the findings from Rogers and Bottomley to test six soils and two manufactured media for MRI suitability. The study was conducted at 4.7 T, while also making note of the water holding capacity, soil texture, and ferromagnetic particle content for each soil. Two of the four soils tested had high ferromagnetic particle concentrations (11.7 and 25.3%) and also had the highest clay content (~25% and 45%, respectively). Clay content was directly related to the ability to image either seminal roots or lateral roots. In those soils with greater clay content, larger seminal roots, but no lateral roots were distinguishable. At low clay content, however, MRI performs quite well. Dusschoten et al. (2016) successfully performed a quantitative analysis of three crop roots using a 4.7 T magnet in a sandy loam with 4% clay content and less than 0.2% ferromagnetic particles by mass.

In all of the experiments described above, the researchers used a HF-MRI unit in a laboratory setting to determine the extent an MRI could image roots in the soil. The higher magnetic field produces a higher spin polarization in the material being studied, which may result in a detected signal with a higher signal-to-noise ratio (SNR), but also will produce image artifacts due to the presence of soil with relatively high magnetic material content. To avoid this issue, researchers created artificial soils with low magnetic material (< 4% by mass) which correlates with relatively low clay contents (~10% or less).

We hypothesize that the operation of an MRI in a low magnetic field regime (LF-MRI) will reduce or remove image distortions, while preserving the ability to use the difference in relaxation times between soil water and root water as a contrast mechanism to allow the separation of their signals. It will enable scientifically-useful images to be obtained in agriculturally relevant soils. We describe four specific experiments that answer the critical questions concerning the implementation of a LF-MRI for root phenotyping.

1) The determination of the NMR properties of soil water and root water at low magnetic fields.
2) The development and testing of a small-scale MRI system operating at 47 mT in four soil types.
3) Determination of the relationship between LF-MRI signal-to-noise-ratio (SNR), image resolution and scanning time at 47 mT field strength for roots in soil.
4) Evaluation of a deep neural network approach (AUTOMAP) to improve SNR and image quality for plant root imaging with LF-MRI

2. Material and methods

2.1. Field sample collection

TX08001, a bioenergy sorghum hybrid (*Sorghum bicolor* (L.) Moench.), was planted on May 30th, 2018 at the Texas A&M AgriLife Field laboratory in Burleson County, Texas USA. Sorghum was planted to a depth of 2.5 cm with a row spacing of 76 cm in two soil types, a Weswood silt loam, (a Udifluventic Haplustept, 25% clay, mixed minerology) and a Belk clay (a Entic Hapludert, 49% clay, mixed minerology) and has a high coefficient of linear extensibility. Standard agronomic practices were employed for fertilization and cultivation. Soil cores containing sorghum roots were collected roughly 120 d after planting from the two field sites.

A hydraulic soil probe (Giddings Machine Company, Inc., Windsor, CO., USA) mounted on a 1-ton pickup truck was used to collect soil cores with a diameter of 5.7 cm. The probe had a polyethylene terephthalate (PETG) sleeve insert allowing the collection and easy removal of the soil core from the probe. The probe was pushed into the ground adjacent to the crown roots on the inner-row side of the sorghum plant to a depth of 30.5 cm. The plastic sleeve was then removed from the metal core with the soil and roots contained inside, and marked to indicate the core's orientation to the plant stalk. Two cores

were collected on either side of a given plant stem, between the rows in both the Weswood silt loam and the Belk clay on each collection day. Each core was cut into a 0-to 7.5-cm and a 7.5- to 15-cm depth section, for a total of four cores representing one plant for each soil type. The cores were treated for fire ants and shipped overnight to ABQMR, Inc., (Albuquerque NM) for laboratory-based LF-MRI imaging where the cores were refrigerated at approximately 8C between imaging sessions.

2.2. Greenhouse sample collection

To test the system in a broader range of soils, rhizotrons (26.1-cm diameter, 75-cm long) were filled with dried ground soil. Either a Houston Black clay soil (52% clay, smectitic minerology, an Udic Haplusterts) which has a high coefficient of linear extensibility, or a sandy loam soil (5–10% clay) purchased from a nearby landscaping supply store was used. Sorghum was planted in the rhizotrons, with cores being collected starting at roughly 90 d after planting. A 6.4-cm diameter soil core was collected to a depth of 37.5 cm. The full core was then cut into five 7.5-cm long sections for imaging and comparison.

2.3. NMR properties of soil and roots

While it is not the goal of this paper to give an in depth description of the physics of an MRI system, we recognize that more background information may be helpful to understand the methods put forth in this paper. The following publications are excellent introductions to the basics of MRI (Brown et al., 2014; Callaghan, 1994; Fukushima and Roeder, 1982; Hornak, 1997).

Soil and root image contrast is determined by the water NMR relaxation times (T_1, T_2) in the target material (roots) and the surrounding background material (soil). In the application of MRI, T_1 determines the maximum rate of repetition of the imaging pulse sequence, while T_2 determines the maximum time after the initial radio frequency (RF) pulse that the signal can be obtained. Our imaging strategy for the root vs soil discrimination is based on the differences in T_2 relaxation time, and therefore measurements of these parameters under realistic conditions is critical.

We used an inversion-recovery sequence with a Carr-Purcell-Meiboom-Gill (CPMG) (Fukushima and Roeder, 1982) read out to measure T_1 and T_2. A custom built 267 mT NMR scanner was used on eight soil samples to explore the usefulness of LF-MRI in soils while the 47 mT scanner (which is discussed later) was being constructed. After construction of the 47 mT system was completed, six soil samples were re-tested to verify that relaxation values were similar between the two systems. A range of clay contents (8–65%) with seven different water contents (0.05–0.35 kg kg^{-1}) were explored. To obtain the range in water content, the soils were air dried, passed through a 2-mm sieve, and wet by weight (with an oven-dry correction). Fifty inversion times from 10 to 100 ms were evenly spaced on a log scale. The repetition time was 200 ms, and 150 echoes were generated at an echo spacing of 120 μs. Depending on moisture content, the number of averages ranged from 4 to 64.

A second experiment was conducted to measure T_1 and T_2 in three samples of approximately 2-mm diameter sorghum roots. The soil was washed off and the roots were placed in a glass container for scanning. We used 40 inversion times from 500 μs to 5 s evenly-spaced on a log scale. The repetition time was 10 s and there were 64 echoes with echo spacing of 10 ms and 4 signal averages.

2.4. 8-cm bore MRI system

An MRI system was designed and built to test the hypotheses that operation at low magnetic field would allow the generation of root images in agricultural soils. A 47 mT electromagnet (corresponding to water NMR frequency of 2 MHz) with an 8-cm bore and 30 cm in length (Fig. 1A) was used to image each soil core. The magnet was wound on an 18-cm outside diameter (OD) nylon cylinder. An electromagnetic system was chosen based on the long term plans for field deployment, where we believe it is advantageous to be able to switch the magnet on and off for safety reasons. The electromagnet main solenoid and end corrections coils were energized by separate power supplies (Hewlett-Packard 6012B) which were operating near their (kw) capacity. This operational capacity was a driving consideration for choosing 47 mT.

An in-house manufactured gradient coil was wound on a 12.5-cm OD polycarbonate cylinder, which was used to spatially encode the roots in a 2-D *k*-space. The 1 kW of heat generated in the 16 AWG wire of the magnet's main windings and end windings was removed by using recirculated hydraulic oil and an oil-to-water heat exchanger (Fig. 1.B). A transmit-receive radio frequency saddle coil was wound on a 11.5-cm OD polycarbonate cylinder and was used to apply the RF pulse and then receive the magnetic resonance signal from the sample. Three AE Techron model 2105 amplifiers (Audio Electronics, Inc., Elkhart IN) were used to drive the three gradient coils, and a single Tomco RF amplifier (Tomco technologies, Stepney, South Australia) was used to generate the RF pulses used to flip the nuclear spins. A Tecmag Redstone console (Tecmag, Houston TX, USA) was used to control the pulse programmer, RF transmitter and receiver, and the gradient system (Fig. 1C). After the construction of the 47 mT scanner, six soils from the above experiment were tested to verify that the relaxation values at 47 mT approximately agreed with those found with the 267 mT scanner.

To demonstrate that a LF-MRI system can be used for visualizing

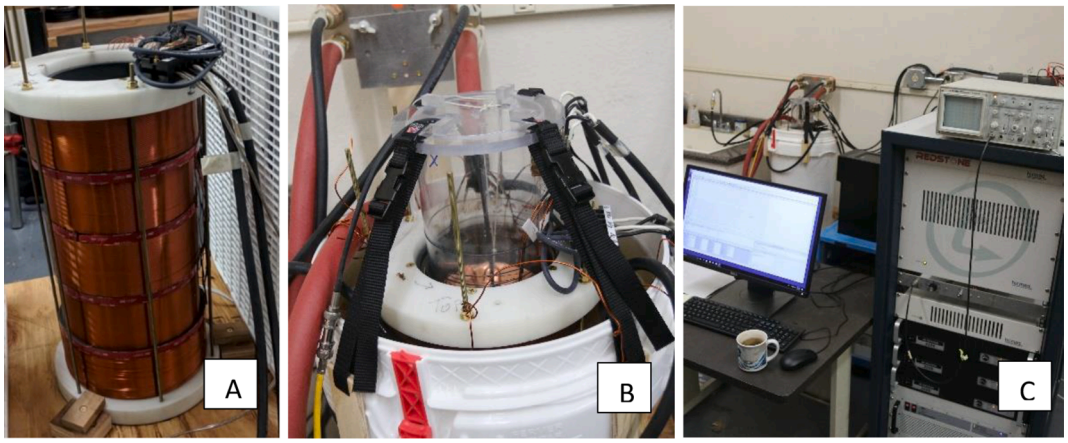

Fig. 1. Image 1.A is the 8-cm bore electro magnet. Image 1.B shows the magnet, RF coil, and gradient coil placed in the cooling oil. Image 1.C shows the Techmag Redstone along with the computer that controls the system.

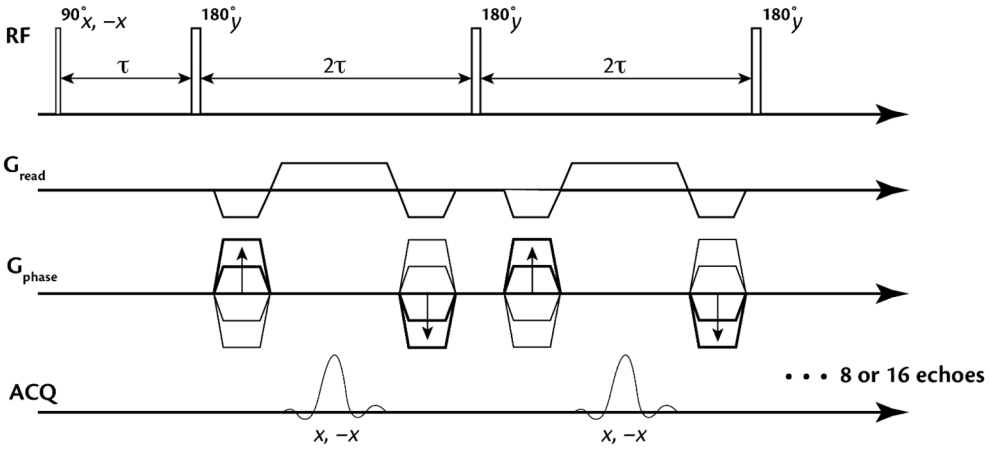

Fig. 2. Pulse sequence for image generation uses CPMG pulse sequence that is fully rewound, both for phase encode and frequency read out. The subscripts refer to the phase of the RF transmit, data acquisition. τ and 2 τ are RF pulse spacing. Depending on the experiment either 8 or 16 echos are acquired and averaged together for each phase encode.

roots in soils, 2-D projection images were acquired from cores collected from two different sources. The field soil cores collected from the Weswood silt loam and Belk clay were used as well as the Houston Black clay and sandy loam rhizotron cores. For these images, a CPMG (Fukushima and Roeder, 1982) sequence was used where each echo is acquired with the same phase encode and read out gradients. This approach allows all of the echos to be averaged to improve the SNR. In this work we leave the third dimension unresolved. Two approaches to the 2-D imaging are reported here, both use the pulse sequence shown in Fig. 2. The first sequence uses eight sequential spin echoes, with an echo spacing of 7 ms and a 2-D projection image acquisition time of 1 h. The second sequence uses sixteen sequential spin echoes with an echo spacing of 7 ms; fewer signal averages were used, so the image acquisition time for each 2-D projection in this experiment was 15 min. For both methods a 0.5 s repetition time was used, along with a field of view of 80 mm. For both approaches, the RF-pulses were rectangular (or "hard") pulses (Hornak, 1997) in time (Fig. 2). Each echo (either eight or sixteen) acquired the same line in *k*-space such that the data were averaged for improved signal-to-noise ratio. These sequences parameters were chosen to produce the best SNR for the system. The timing implies that soil water signals ($T_2 < 4$ ms) were heavily suppressed while the root water signals ($T_2 \sim 100$ ms) were only slightly attenuated, resulting in root images that are T_2-weighted.

The time domain *k*-space data was appended with zeros (known as zero -filling) to create an interpolated image of a standard size regardless of the pixel resolution. For the experiments described here, the acquired *k*-space matrix sizes which range from 48 × 48 to 92 × 92 (the second number is the number of phase encode steps) being zero filled and transformed to create images that are 128 × 128 pixels. The images were reconstructed from *k*-space using the conventional Inverse Fast Fourier Transform (IFFT), or with AUTOMAP.

2.5. SNR, resolution, scanning time

To explore the relationship between image resolution, image acquisition time and signal-to-noise ratio (SNR) one Weswood silt loam core and one Belk clay core were imaged six times each. For both soil types, two sets of 2-D projection images are generated with a fixed field of view of 80 mm. For the first set of experiments, the scanning time was fixed and the resolution was changed from 1.74, 1.25, and 0.625 mm pixel^{-1}, which causes the image SNR to change in response. For the second set of experiments the images were acquired at the same spatial resolutions as before; however the image acquisition times were increased accordingly to deliver a nearly constant SNR. The data were zero filled as described above, resulting in images that are 128 × 128 pixels.

2.6. Automap

Low field MRI generally suffers from low SNR due to the intrinsically low Boltzmann spin polarization. As a result, relatively long acquisition times are needed to accommodate the additional signal averaging required to attain sufficient SNR. Zhu et al. (2018) have recently described a deep-neural-network-based approach for image reconstruction known as Automated Transform by Manifold Approximation (AUTOMAP). It leverages data-driven learning of the low-dimensional manifold representations of real-world data that are robust to corruptions, such as noise, and have been shown to improve imaging performance. This method is applied to the raw data in *k*-space and is used to transform the MRI data to image space.

We assessed the performance of AUTOMAP reconstruction to improve the imaging quality of the LF-MRI system. The image SNR was used to compare AUTOMAP reconstruction of the same 2-D LF-MRI data with the more conventional inverse fast fourier transform reconstruction method. Six images corresponding to three soil types were reconstructed at resolutions of 1.67, 1.11, and 0.83 mm pixel^{-1}.

AUTOMAP was trained on the Fourier forward-encoding model using a training corpus assembled from 55,000 2-D synthetic roots images. These root images were generated using a 3D root system growth model implemented in MATLAB- called RootBox (Dunbabin et al 2013). Random additive white gaussian noise was applied to each image in the training set to expedite manifold learning during training. To produce the corresponding *k*-space representations for training, each noise-corrupted image was Fourier Transformed with MATLAB's native 2-D FFT function. The neural network was trained from the noise corrupted *k*-space encodings and target 'noise-free' images to learn an

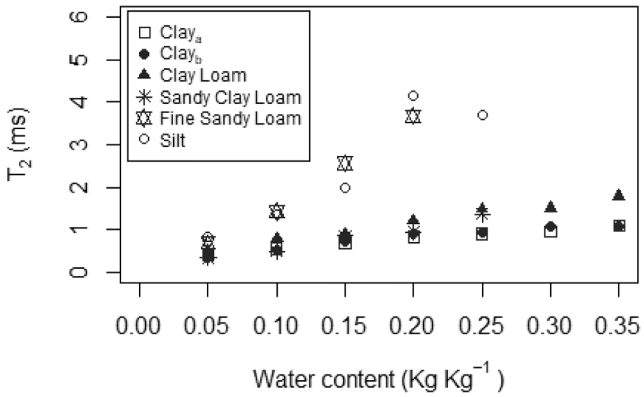

Fig. 3. Measured soil water T_2 versus water content for six soils with different texture classes. As water content increases, the relaxation times also increase. T_2 also varies between textures.

Table 1
A summary of the soil particle size distribution for nuclear magnetic resonance relaxation times (T_1 and T_2). N/A represents a soil water content that was not achievable because it is beyond the liquid limit for that soil.

	Particle size distribution			Relaxation times at 0.1 kg kg^{-1} water		Relaxation times at 0.25 kg kg^{-1} water	
Texture class	Sand %	Silt	Clay	T_1 ms	T_2	T_1	T_2
$Clay_a$[†]	3.1	33.5	63.4	0.98	0.55	1.61	0.90
Silty Clay	3.0	44.3	52.7	0.88	0.47	1.60	0.88
$Clay_b$[†]	8.6	39.4	52.0	0.74	0.52	1.31	0.94
Clay Loam	32.5	34.0	33.5	1.3	0.77	2.46	1.47
Silty Clay Loam	15.2	56.1	28.7	1.32	0.70	2.37	1.31
Sandy Clay loam	55.7	14.5	21.8	1.3	0.49	3.95	1.37
Fine Sandy Loam	69.8	20.4	9.8	2.37	1.42	N/A	N/A
Silt	3.0	89.1	7.9	3.01	1.37	7.97	3.7

[†] $Clay_a$ has mixed mineralogy; $Clay_b$ has smectitic mineralogy.

optimal feed-forward reconstruction of *k*-space domain into the image domain. The network architecture described in Zhu et al. (2018) was used in this experiment. The raw 2-D *k*-space datasets from all samples were stacked and multiplied by a scalar so the range of signal intensities lies within that of the corresponding training models. The stacked *k*-space datasets were then reconstructed with the trained model. The signal magnitude of each 2-D dataset was normalized to unity to enable fair comparison between both reconstruction methods. SNR was then computed by dividing the signal magnitude by the standard deviation of the noise.

3. Results & discussion

3.1. NMR properties of soil and roots

We found a large difference between the NMR T_2 relaxation times of soil water in the eight soils tested (Fig. 3) and in roots. An increase in the relaxation time corresponds with an increase in the water content for all soils tested; however, the rate of increase with water content is dependent on soil type. Relaxation times of soil water are strikingly short when compared to free water or root water, leading us to conjecture a relaxation mechanism where the ^1H nuclei interact with paramagnetic ions in the soil. As soil water content increases, the soil surface area is unchanged, leaving increasing amounts of free water in the soil matrix. Hence surface-bound water becomes a smaller fraction of the total soil water. This indicates that in this system, the water relaxation is dominated by the surface bound water interacting with soil paramagnetism. This results in the relaxation time for water in a soil increasing as the amount of soil water increases; however, proving this hypothesis requires further research. The measured T_2 relaxation in soil water as a function of soil water content is plotted in Fig. 3.

The T_2 relaxation time for the soil water across the tested soils ranged from 0.33 to 4.14 ms, and T_1 ranged from 0.51 to 9.54 ms (Table 1). Soil water contents ranged from permanent wilting point to field capacity for each soil, as a representative range of possible water contents in the field. In contrast, the T_1 relaxation time for water in bare roots was between 0.7 and 1.2 s, and the T_2 relaxation time of water in bare roots ranged from 85 to 140 ms. By adjusting the NMR echo time in the LF-MRI pulse sequence such that it is long in comparison to T_2 of soil water and short in comparison to T_2 of root water, we are able to image the root water without signal contamination from soil water.

3.2. Imaging system

A critical step for this work is the development and testing of a LF-MRI system capable of producing images of roots in agricultural soils. Fig. 4 shows 2-D projection images, acquired in the 8-cm bore system, of field-collected, intact cores. Fig. 4A shows roots in the Weswood soil (25% clay), and Fig. 4B shows root in a Belk clay (49% clay). Both images are 2-D projections of cores that are the top 0 to 7.5 cm depth.

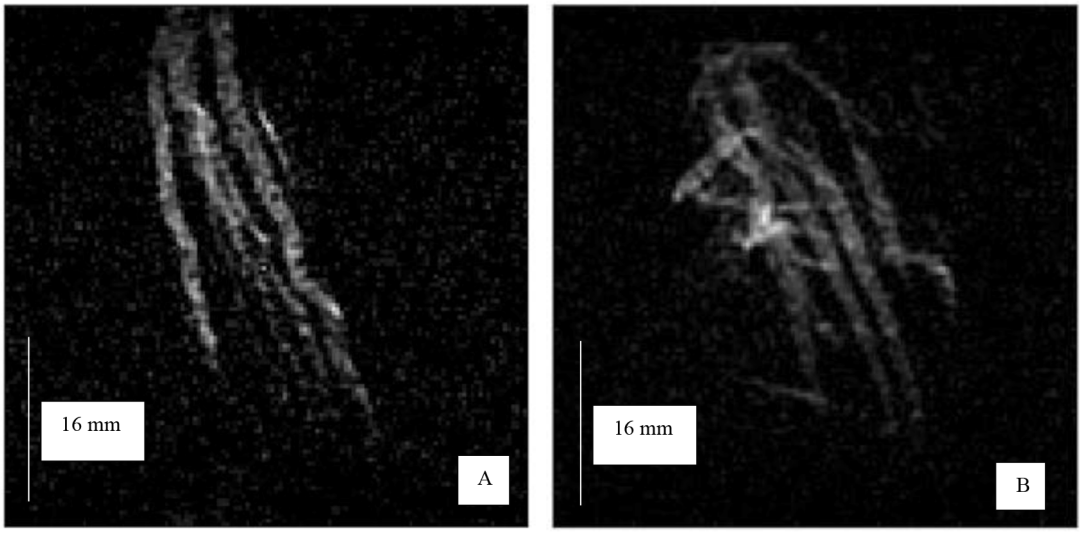

Fig. 4. Energy sorghum root images acquired in the 8-cm LF-MRI scanner. Roots shown in this image are nodal roots that are 1.5–2.0 mm in diameter. Both images are of intact soil cores collected at 0–7.5 cm depth, have a resolution of 0.8 mm, and an acquisition time of 1 h. Image A) is a Weswood silt loam and B) is a Belk clay; both are collected adjacent to the plant.

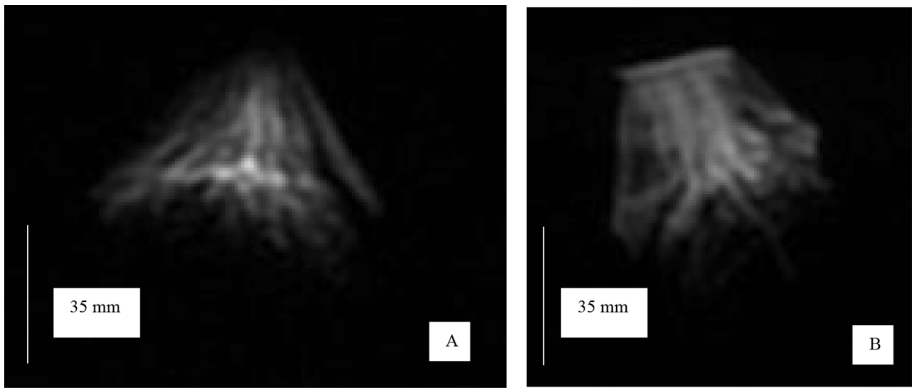

Fig. 5. A) LF-MRI of the root crown from a rhizotron-grown greenhouse sorghum in a Houston Black and B) manufactured sandy loam soil. The plants were harvested approximately 90 days after planting. The roots seen in these images are 1.5–2.0-mm in diameter. These images are 2-D projection, with an image acquisition time of 15 min and a pixel resolution of 1.74.

The images have a resolution of 0.8 mm pixel^{-1} using a scan time of 1 hr. The roots shown here are nodal roots of sorghum that are between 1.5 and 2.0 mm in diameter. In this projection image some of the brighter pixels represent one or more roots crossing each other.

2-D projection images acquired in the 8-cm bore LF-MRI scanner of soil and root cores from the rhizotrons are shown in Fig. 5. These images were acquired with a 15-min scanning time and pixel size of 1.74 mm. Fig. 5A shows a full root crown in a Houston black clay rhizotron. Fig. 5B shows a similar root crown grown in a sandy loam rhizotron. When Fig. 5A and B are compared, one can see different rooting structures that are likely the result of soil type, as all other environmental factors were similar. The apparent blurring in Fig. 5 is due to the relatively low image resolution combined with the visualization of 3-D information in a 2-D projection image.

Experimental results in Figs. 4 and 5 demonstrate that we can generate 2-D projection images of roots with a diameter of 1.5 mm or larger, in moderate to heavy clay soils using this LF-MRI system with relatively short image acquisition times of 15–60 min. Increased signal averaging obtained through longer acquisition times generates higher SNR and will allow smaller roots to become visible in the images. The images presented in Figs. 4 and 5 are reconstructed using the IFFT method.

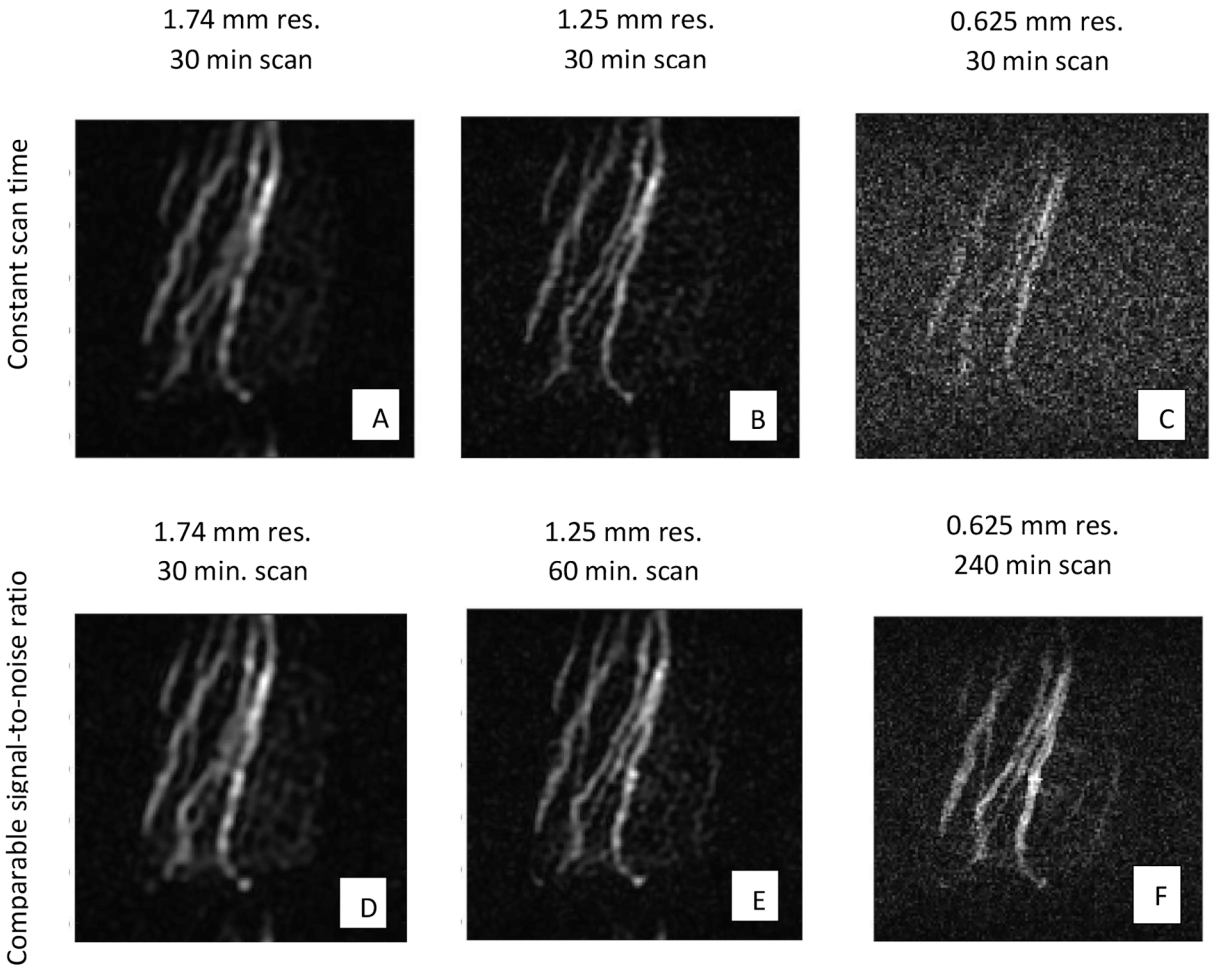

Fig. 6. LF-MRI images of sorghum roots in a Weswood silt loam soil core, all with a fixed FOV of 80 mm. Images (A–C) were acquired in 30 min, with the indicated image resolution, leading to differences in image SNR. Images (D–F) were acquired with acquisition time chosen to maintain image SNR, with longer acquisition times needed for higher resolution imaging.

3.3. SNR, resolution, scanning time

To develop a successful imaging protocol, the relationship between SNR, image acquisition time, and resolution must be determined. Fig. 6(A–C) shows an image collected of a Weswood silt loam core, with nodal roots ranging from 1.5 to 2.0 mm in diameter. While holding the image acquisition time constant at 30 min and setting the image pixel size at 1.74, 1.25, and 0.625 mm pixel^{-1}, the SNR changes in response. The resulting SNR becomes smaller (worse) as the pixels become smaller, making it harder to identify roots in the image. Fig. 5(D–F) show the same roots, but here the SNR is held constant as the resolution is changed from 1.74, to 1.25 and 0.625 mm pixel^{-1} and the acquisition time is increased from 0.5 to 4 hrs.

Fig. 7 shows a similar relationship for a Belk clay soil core, confirming the conclusion that the resolution and SNR are inversely related for a constant scan time. Likewise, resolution and scan time are inversely related for a constant SNR, and none of these properties are related to the soil texture. These experiments indicate that for a successful imaging sequence we will need to balance resolution, SNR, and image acquisition time to create a practical field-based imaging system that creates useful images in a reasonable time frame.

3.4. AUTOMAP image reconstruction

AUTOMAP reconstruction versus conventional IFFT reconstruction method of roots images is shown in Fig. 8 for two Belk clay soils. Images acquired with a matrix size of 48 × 48 (spatial resolution of 1.67 mm) showed an improvement in the mean SNR of 69% and 29% compared to the standard IFFT method. The noise levels in these images are lower by more than 30%, giving the roots architecture better contrast with the MR signal from the soil.

For the 72 × 72 matrix size (1.11 mm spatial resolution) root images from Houston Black clay (Fig. 8E–F) and from the sandy loam (Fig. 8G and H), where the SNR of the standard IFFT image was high, showed improvements of 161 and 148%, respectively.

For the 96 × 96 matrix size (spatial resolution of 0.83 mm) root images collected from Houston Black clay (Fig. 8I and J) show a mean SNR improvement of 171%. The same images shown in Fig. 8 (K and L) with a lower window level, reveal the significant noise floor reduction when the data is reconstructed with AUTOMAP.

For the 128 × 128 matrix size (spatial resolution of 0.63 mm), the root images reconstructed with AUTOMAP not only show an improvement of 88% in mean SNR but also the removal of spike artifacts

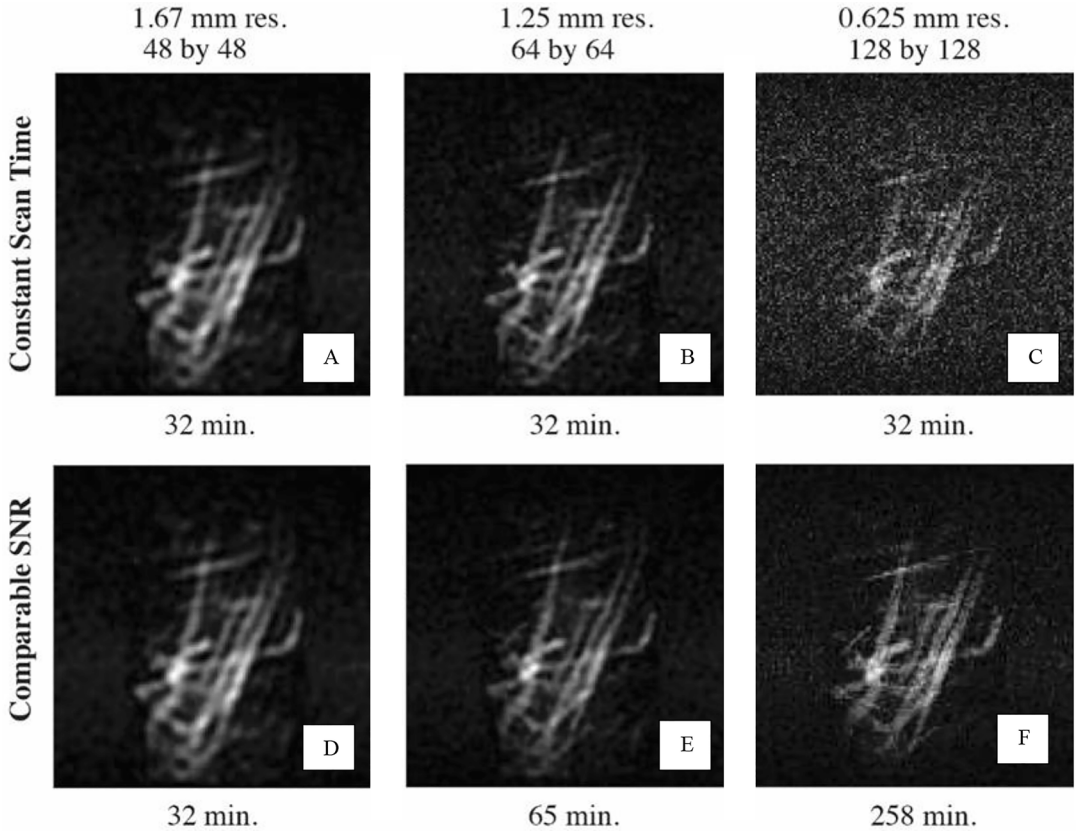

Fig. 7. LF-MRI images of sorghum root in a Belk clay soil core, all with a fixed FOV of 80 mm. Images (A–C) were acquired in 32 min, with the indicated image resolution leading to different SNR. Images (D–F) were acquired by selecting image acquisition times that allowed the SNR to remain constant resulting in longer acquisition times for each improvement in image resolution.

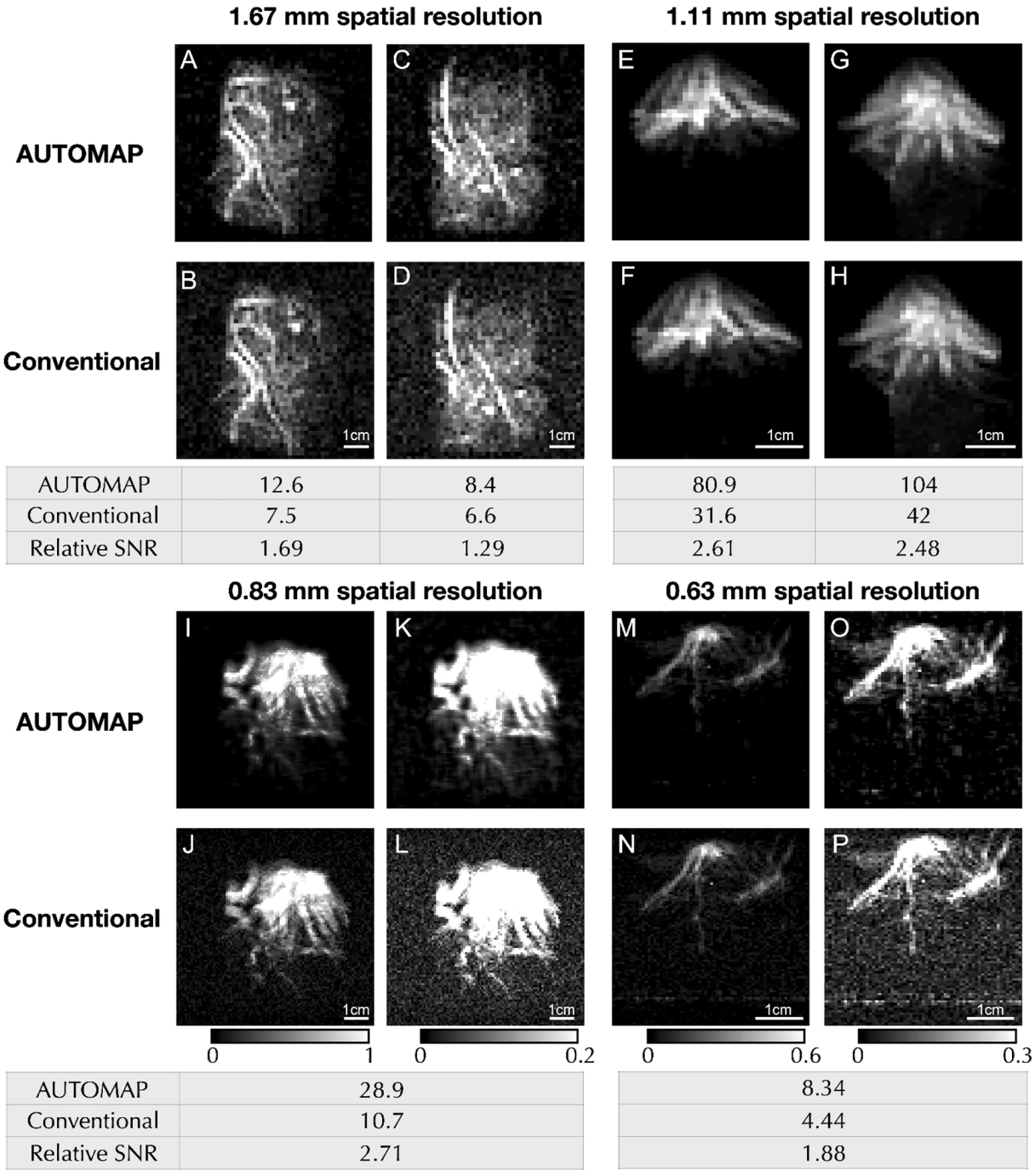

AUTOMAP	12.6	8.4	80.9	104
Conventional	7.5	6.6	31.6	42
Relative SNR	1.69	1.29	2.61	2.48

AUTOMAP	28.9	8.34
Conventional	10.7	4.44
Relative SNR	2.71	1.88

Fig. 8. AUTOMAP versus Conventional IFFT reconstruction method of roots images – Four spatial resolutions are shown – 1.67 mm pixel size (A–D), 1.11 mm pixel size (E–H), 0.83 mm pixel size (I–L) and 0.63 mm pixel size (M–P). For each set of spatial resolutions the top images were reconstructed using AUTOMAP and the bottom images were reconstructed using the conventional IFFT method. Images (I and J) were windowed to a lower level in images K and L respectively, to show the decrease in noise. Likewise the images (M and N) were windowed to a lower level in images (O and P) respectively, to show the noise reduction and spike elimination. For each figure, image intensities are displayed in a windowed range of intensities (from 0 to 1), as indicated on the legend. The table indicates the image SNR for both reconstruction approaches and tabulates the fractional SNR enhancement seen with AUTOMAP.

(Fig. 8M and N). As seen in the windowed images in Fig. 8O and P, the RF leakage artifact (horizontal streak near bottom) was significantly eliminated with AUTOMAP reconstruction.

The improved contrast in roots, reduction of noise, and spike artifact elimination indicate the utility of AUTOMAP. The lowering of the noise floor, and the improvement to the SNR allows the user greater latitude to adjust the scanning time, resolution or SNR by providing a greater range post hoc.

4. Conclusion

Visualization and measurement of root structure *in situ* would aid in understanding the function of roots and how roots behave under different environmental conditions. We have demonstrated that low field MRI can allow scientists to detect and visualize roots through intact, natural soils and collect spatial information to aid in understanding root morphology, architecture and development. While previous studies have shown the difficulty of using high field MRI and soils with high

clay content (> 10%), these issues are less problematic when using low field MRI.

We have demonstrated that the soil water signal relaxation time T_2 is much shorter than root water signal (4 ms vs. 120 ms), allowing soil water signals to be suppressed, resulting in images of roots in the soil. We have measured the clay content and have shown that LF-MRI is still successful in situations with moderate to high clay content. We have shown that images can be collected in soils with more than 10% clay content. The images shown in this paper demonstrate that there is a balance of scanning time, SNR, and resolution to be optimized. We have also demonstrated that AUTOMAP can be used to improve the SNR (by 29–148%) and lower the noise floor during the image reconstruction stage, allowing for more flexibility in the application of a LF-MRI system.

The next step in our research is to develop an LF-MRI system that can be deployed in the field. It is ideal to be able to image lateral roots that have smaller diameters in addition to the larger diameter nodal roots. For imaging smaller roots, we will need to improve the SNR, which will be done by further improvements to the hardware, software, and by continuing to explore the use of AUTOMAP. To continue this research in the field, the system will be scaled up. It is our goal to increase the linear size of the magnet by a factor of three; we expect to be able to generate a 1.5 mm resolution image in approximately 25 min.

Declaration of Competing Interest

The authors declare the following financial interests/personal relationships which may be considered as potential competing interests: Our only conflict of interest for this manuscript is that Cristine L. S. Morgan is one of the editor-in-chief of Geoderma.

Acknowledgments

The information, data, or work presented herein was funded in part by the Advanced Research Projects Agency-Energy (ARPA-E), U.S. Department of Energy, under Award Number DE-AR0000823. The views and opinions of authors expressed herein do not necessarily state or reflect those of the United States Government or any agency thereof.

References

Araujo, A.P., Fernades, A.M., Kubota, F.Y., Brasil, F.C., Teixeira, M.G., 2004. Sample size for measurement of root traits on common bean by image analysis. Pesquisa Agropecuaria Bras. 39, 313–318.

Armengaud, P., Zambaux, K., Hills, A., Sulpice, R., Pattison, P.J., Blat, M.R., Amtmann, A., 2009. EZ-Rhizo: integrated software for the fast and accurate measurement of root system architecture. Plant J. 57, 945–956.

Atkinson, J.A., Pound, M.P., Bennett, M.J., Wells, D.M., 2019. Uncovering the hidden half of plants using new advances in root phenotyping. ScienceDirect 55, 1–8.

Brown, R., Cheng, Y., Haacke, M., Thompson, M., Venkatesan, R., 2014. Magnetic Resonance Imaging: physical principles and sequence design, Second Edition. Wiley and Sons.

Callaghan, P., 1994. Principles of Nuclear Magnetic Resonance Microscopy. Oxford University Press, Oxford, New York.

Dunbabin, V., Postma, J., Schnepf, A., Pagès, L., Javaux, M., Wu, L., Leitner, D., Chen, Y., Rengel, Z., Diggle, A., 2013. Modelling root-soil interactions using three-dimensional models of root growth, architecture and function. Plant Soil 372, 93–124.

Dusschoten, D., Metzner, R., Kochs, J., Postma, J.A., Pflugfelder, D., 2016. Quantitative 3D analysis of plant roots growing in soil using magnetic resonance imaging. Plant Physiol. 170, 1176–1188.

Flavel, R.J., Guppy, C.N., Tighe, M., Watt, M., McNeill, A., Young, I.M., 2012. Non-destructive quantification of cereal roots in soil using high-resolution x-ray tomography. J. Exp. Bot. 63, 2503–2511.

Flavel, R.J., Guppy, C.N., Rabbi, S.M., Young, I.M., 2017. An image processing and analysis tool for identifying and analyzing complex plant root systems in 3-D soil using non-destructive analysis: Root1. PLoS ONE 10, 1–18.

Fukushima, E., Roeder, S.B.W., 1982. Experimental PULSE NMR: A Nuts and Bolts Approach. CRC press, Boco Raton.

Hall, L.D., Agmin, M.H.G., Sanda, M., Votrubova, J., Richards, K.S., Chorley, R.J., Cislerova, M., 1997. MR properties of water in saturated soils and resulting loss of MRI signal in water content detection at 2 tesla. Geoderma 80, 431–448.

Hornak, J. P., 1997. The Basics of NMR. https://www.cis.rit.edu/htbooks/nmr/index.html.

Jahnke, S., Menzel, M.I., Dusschoten, D., Roeb, G.W., Buhler, J., Minwuyelet, S., Blumler, P., Temperton, V.M., Hombach, T., Streun, M., Beer, S., Khodaverdi, M., Ziemons, K., Coenen, H.H., Schurr, U., 2009. Combined MRI-PET dissects dynamic changes in plant structures and functions. Plant J. 59, 634–644.

Koch, A., Meunier, F., Vanderborght, J., Garre, S., Pohlmeier, A., Javaux, M., 2019. Functional-structural root system model validation using a soil MRI experiment. J. Exp. Bot. 70, 2797–2809.

Lafond, J.A., Han, L., Duiteul, P., 2015. Concepts and analyses in the CT scanning of root systems and leaf canopies: a timely summary. Front. Plant Sci. 6, 1–7.

Lynch, J., 1995. Root architecture and plant productivity. Plant Physiol. 109, 7–13.

Lynch, J.P., 2018. Rightsizing root phenotypes for drought resistance. J. Exp. Bot. 69, 3279–3292.

Metzner, R., Dusschoten, D., Buhler, J., Schurr, U., Jahnke, S., 2014. Belowground plant development measured with magnetic resonance imaging (MRI): exploiting the potential for non-invasieve trait quantification using sugar beet as a proxy. Front. Plant Sci. 5, 1–11.

Mooney, S.J., Pridemore, T.P., Helliwell, J., Bennett, M.J., 2012. Developing x-ray computer tomography to non-invasively image 3-D root system architecture in Soil. Plant Soil 352, 1–22.

Pflugfelder, D., Metzner, R., Dusschoten, D.V., Reichel, R., Jahnke, S., Koller, R., 2017. Non-invasive imaging of plant roots in different soils using magnetic resonance imaging (MRI). Plant Methods 13, 1–9.

Prebble, R.E., Currie, J.A., 1970. Soil Water measurement by a row resolution nuclear magnetic resonance technique. J. Soil Sci. 21, 273–288.

Rogers, H.H., Bottomley, P.A., 1987. In situ nuclear magnetic resonance imaging of roots: influence of soil type, ferromagnetic particle content, and soil water. Agron. J. 79, 957–965.

Trachsel, S., Kaeppler, S.M., Brown, K.M., Lynch, J.P., 2011. Shovelomics: high throughput phenotyping of maize (Zea mays L.) root architecture in the field. Plant Soil 341, 75–87.

Votrubova, J., Sanda, M., Cislerova, M., Amin, M.H.G., Hall, L.D., 2000. The relationship between MR parameters and the water content in packed samples of two soils. Geoderma 95, 267–282.

Xhou, X., Luo, X., 2009. Advances in non-destructive measurement and 3-D visualization methods for plant roots based on machine vision. 2009 2nd International Conference on Biomedical Engineering and Informatics. Tianjin, China. DOI: 10.1109/BMEI.2009.5304876.

Zhu, B., Liu, J.Z., Cauley, S.F., Rosen, B.R., Rosen, M.S., 2018. Image reconstruction by domain-transform manifold learning. Nature 555, 487–492.

Zhu, J., Ingram, P.A., Benfey, P.N., Elich, T., 2011. From lab to field, new approaches to phenotyping root system architecture. ScienceDirect. 14, 310–317.